Kinetic Controls on Cu and Pb Sorption by Ferrihydrite

ANDREAS C. SCHEINOST,*,† SVEN ABEND,‡ KAUMUDI I. PANDYA,§ AND DONALD L. SPARKS†

Department of Plant and Soil Sciences, University of Delaware, Newark, Delaware 19717, Department of Physics and Astronomy, SUNY Stony Brook, New York 11794, and National Synchrotron Light Source, BNL, Upton, New York 11973

Metal partitioning in ferrihydrite suspensions may reach equilibrium only after a long reaction time. To determine key factors controlling the kinetics, we measured Cu and Pb uptake as a function of ferrihydrite morphology, reaction temperature, metal competition, and fulvic acid concentration over a period of 2 months. X-ray microscopy, which was used to probe ferrihydrite morphology in suspension, showed that drying irreversibly converted the gellike structure of fresh precipitate into dense aggregates. These dense aggregates sorbed Cu and Pb much slower than the gel. Temperature had a more pronounced effect on the kinetics of metal uptake by ferrihydrite gel than by dense ferrihydrite. Independently of treatment and time, Cu and Pb were bound to the ferrihydrite surface by formation of edge-sharing inner-sphere sorption complexes as confirmed by X-ray absorption fine-structure (XAFS) spectroscopy. This invariable binding mechanism, together with the observed effects of morphology and temperature, are in line with surface diffusion limiting the slow sorption process. The quantification of diffusion-limited surface sites in soils and sediments and the subsequent estimation of the effect of reaction time and temperature will be a challenge for properly predicting the fate of metals in the environment.

Introduction

Ferrihydrite is one of the most important sorbents in soils, sediments, and water bodies and is frequently used for wastewater treatment (*1*, *2*). Although the mineral is metastable and converts into more stable iron (hydr)oxides such as goethite and hematite, it is constantly re-created by microbially mediated redox cycles. Furthermore, its conversion is slow at temperatures below 20 °C (*3*) and further retarded by adsorbed organic and inorganic species (*4*−*7*). Its sorption capacity is due to highly reactive surface sites (*8*) and a surface area ranging from 200 to 800 m^2/g depending on the method of determination (*9*). Sorption densities close to 1 mol of sorbate per mole of ferrihydrite-Fe have been measured (*9*, *10*), suggesting that the surfaces of primary particles with diameters of only a few nanometers are accessible even after aggregation (*11*, *12*).

* Corresponding author's present address: Swiss Federal Institute of Technology, Department of Environmental Sciences, Grabenstrasse 2, CH-8952 Schlieren, Switzerland; phone: (41) 1 633−6147; fax: (41) 1 633 1118; e-mail: scheinost@ito.umnw.ethz.ch.

† University of Delaware.

‡ SUNY Stony Brook.

§ BNL.

A range of metals sorb onto ferrihydrite by formation of inner-sphere sorption complexes, as verified for Cr (*13*), As (*10*, *14*), Se (*15*), and Cd (*16*). Pressure-jump studies showed that this process is generally completed within seconds (*17*−*19*). Despite this fast chemical reaction, sorption frequently increased over days or even months (*20*). For phosphate sorption, Van Riemsdijk and co-workers (*21*) suggested that this slow sorption step could be due to the formation of surface coatings on metal oxides which act as a diffusional barrier for further phosphate sorption. Similarly, slow sorption of Cd has been explained by an ongoing precipitation reaction of Cd hydroxide (*22*). Furthermore, slow sorption may be caused by the transformation of the sorbent ferrihydrite into the more stable iron oxides goethite or hematite (*23*−*25*).

However, slow sorption has also been observed when precipitation reactions and ferrihydrite transformations could be excluded by spectroscopic methods. Fuller et al. (*26*) found a slow sorption reaction for arsenate on ferrihydrite, where formation of inner-sphere sorption complexes was the only binding mechanism, as verified by XAFS. The authors suggested that the slow sorption might be due to surface diffusion into the spongelike interior of either ferrihydrite aggregates or the branched structure of primary ferrihydrite particles. Consequently, they fitted the kinetics data with a numerical model describing intraparticle diffusion into the pore system of a spherical particle. Axe and Anderson (*27*, *28*) employed analytical solutions for spherical diffusion to fit the kinetics of Sr and Cd uptake by ferrihydrite. Using experimental values for aggregate size distribution and shape, porosity, and site density, they found a good agreement between model and data. Besides these modeling approaches, Willet and co-workers (*29*) found microscopic evidence for diffusion of phosphate into the interior of ferrihydrite aggregates over a time scale of days while the sorption mechanism remained unchanged as confirmed by infrared spectroscopy.

Due to the multitude of processes explaining slow sorption by ferrihydrite, there still remains some uncertainty on the extent of surface diffusion and its importance in natural systems. The intention of our study was to quantify and explain the long-term sorption kinetics of Cu and Pb on ferrihydrite under experimental settings relevant for soils and sediments. For this objective we modified four variables. First, we studied the sorption of Pb and Cu by two types of sorbents, a fresh precipitate of ferrihydrite and a previously freeze-dried ferrihydrite. We anticipated that drying would produce denser aggregates with less easily accessible interior sites (*30*). Second, we investigated the sorption kinetics at two temperatures, 6 and 24 °C, which may cover a range of common soil and aquifer temperatures. Third, we studied the sorption of Pb in the presence and absence of Cu, and vice versa, to investigate the effect of metal competition on the long-term sorption kinetics. Fourth, we sorbed fulvic acid on to ferrihydrite prior to studying the metal sorption to simulate the influence of ubiquitous dissolved organic carbon.

Experimental Methods

Ferrihydrite Preparation. ACS reagent-grade chemicals, ultrapure water (Micropore SA), and acid-washed polypropylene reaction vessels were used throughout this work. Ferrihydrite was synthesized following the procedure of Schwertmann and Cornell (*31*). After precipitation, the ferrihydrite gel was repeatedly washed with water, after the final centrifugation thoroughly re-suspended by sonification,

10.1021/es000107m CCC: $20.00
Published on Web 00/00/0000

and used within 2 days. Alternatively, the washed ferrihydrite gel was shock-freezed in liquid nitrogen and freeze-dried. This ferrihydrite, called "dense" in the following, was kept in a desiccator and used for the sorption experiments within 1 month. All samples were two-line ferrihydrite according to their X-ray diffraction pattern. The nitrogen BET surface area of various samples at the beginning and end of the kinetics studies was 245 ± 10 m^2/g.

Batch Sorption Kinetics. Sorption studies were performed at pH 5 using a ferrihydrite concentration of 5 g/L and a background electrolyte of 0.1 M $NaNO_3$. The suspensions were stirred at 500 rpm under N_2 atmosphere to exclude CO_2. The temperature of the reaction vessels was adjusted by a water bath at either 24 ± 0.2 or 6 ± 0.2 °C. The pH was adjusted to 5.000 ± 0.005 at least 15 min prior to sorbate addition using a pH stat apparatus (Radiometer) and 0.1 M HNO_3. At $t = 0$, we added 1 mL of 0.1 M $Cu(NO_3)_2$ and/or 1 mL of 0.1 M $Pb(NO_3)_2$. The pH of 5.0 was readjusted first manually and then by the automatic buret using 0.1 M NaOH. Autotitrator settings were determined in preliminary experiments to reach the target pH of 5.0 within 5 min from the acidic side, i.e., without overshooting. After 5 min, the pH deviated by less than ±0.005 units. Samples were taken with a syringe after 5, 10, 20, and 60 min and filtered through 0.2-μm Supor −200 filters (Gelman). The first 0.5 mL of the filtrate was discarded due to potential sorption of metals by the filter. The remaining filtrate was acidified, and [Cu] and [Pb] were determined by atomic absorption spectroscopy (Perkin-Elmer Analyst 800). Further samples were taken in increasing time steps over the next 2 months. After 2 days, the samples were transferred to an orbital shaker in a temperature-controlled chamber (24 ± 2, 6 ± 2 °C). The pH was adjusted in increasing time steps from 24 h in the beginning to 7 days toward the end of the kinetic study. During this period, deviations from the target pH were less than 0.05 units. The amount of metals sorbed was calculated from the difference between initial and final solution concentrations. Batch sorption studies with dense ferrihydrite were conducted in the same way with the following exceptions: the freeze-dried ferrihydrite was rehydrated in 0.1 M $NaNO_3$ for at least 12 h under vigorous stirring, and the pH was adjusted for at least 4 h prior to metal addition to account for slow proton buffering. In most experiments, 1 mM Cu^{2+} *and* 1 mM Pb^{2+} were added simultaneously. A few time series were conducted with either 1 mM Cu^{2+} *or* 1 mM Pb^{2+} to check for competitive effects. To investigate the influence of fulvic acid on the sorption kinetics, 100 mg/L Suwannee River Fulvic Acid Standard (IHSS) was added to the ferrihydrite suspensions adjusted to pH 5.000 and equilibrated for 12 h prior to the sorption experiments. The final concentrations in solution were between 5 and 30 mg C/L, thus within the range observed in soils (*32*−*34*).

Scanning Transmission X-ray Microscopy. Imaging of ferrihydrite suspensions was performed using the STXM at beamline X-1A, NSLS, Upton NY (*35*). The focal optics was equipped with a 160-μm Fresnel zone plate with a focal length of 2.4 mm and a resolution of 35 nm (*36*). To enable the imaging of specimen in a thin water film, a wet cell has been developed by Neuhäusler et al. (*37*). This cell essentially consists of two 100 nm-thick silicon nitride windows enclosing a water film of about 1 μm, which is transmissible for X-rays from 284 to 543 eV. Ferrihydrite suspensions were prepared as described above for the sorption studies. The images were taken at 290 eV at the carbon *K* absorption edge, which yielded a good contrast of ferrihydrite.

X-ray Absorption Fine-Structure Spectroscopy. Copper-K and Pb−L_{III} edge XAFS spectra were collected at beamline X-11A, NSLS. At the Cu edge, 30 spectra were collected to 13 $Å^{-1}$ in fluorescence mode using a 13-element solid-state detector. We placed four sheets of aluminum foil between the sample and detector to reduce the high background fluorescence from Fe. At the Pb edge, 10 fluorescence spectra were collected to 12 $Å^{-1}$ using a Kr-filled Lytle detector and an As-3 μm filter. The samples were mounted in aluminum sample holders as wet pastes and kept moist by sealing with Mylar tape. All spectra were collected at room temperature. Samples were either prepared at the beamline to minimize aging effects (reaction times < 24 h) or stored at 4 °C for a maximum of 5 days before analysis (reaction times > 24 h). All steps of the XAFS data reduction were performed with the WinXAS 97 1.3 software package (*38*) using standard procedures. Theoretical scattering paths were calculated with FEFF 7.02 (*39*) using the structure of Cu(II) hydroxide (*40*) with partial Fe-for-Cu substitution and the structure of red tetragonal Pb(II) oxide (*41*) with partial Fe-for-Pb substitution. Fits were performed in *R* space.

Results and Discussion

Ferrihydrite Morphology. The STXM images of ferrihydrite suspensions reveal two completely different types of morphology. Ferrihydrite, which has been continuously stored in water after precipitation, is shown in parts A and B of Figure 1. The aggregates have a mean diameter of 30 μm as determined by laser diffraction, thus exceeding the cross section of the shown images. Transmitting X-rays are only partly absorbed by the gel, hence modulating regions of varying Fe density. Transitions between water (the brightest regions) and the ferrihydrite aggregates are smooth. The cloud-like morphology is consistent with a ferrihydrite gel with low Fe and high water content. In comparison, the aggregates of dried ferrihydrite were smaller with a mean diameter of 15 μm. Parts C and D of Figure 1 show two aggregates of irregular shape and 3−5 μm in diameter. Large portions of the aggregates are opaque. Since imaged aggregates >1 μm in lateral dimensions may have a thickness close to 1 μm perpendicular to the image due to the spatial limitation imposed by the two silicon nitride windows, this opaqueness clearly indicates that the dried samples have a much higher aggregate density than the ferrihydrite gel. In addition to the larger-sized aggregates, both types of ferrihydrite have smaller aggregates 0.2−0.4 μm in diameter with intermediate density.

The different morphologies of ferrihydrite gel versus dried and then rehydrated ferrihydrite are consistent with the findings of Bottero et al. (*30*). The low density of the aggregates of ferrihydrite gel measured by STXM, together with fractal dimensions below 2 measured for primary ferrihydrite particles by other authors (*42*), suggest that the gel has open, easily accessible surfaces. The open structure of ferrihydrite gel is promoted by the high ionic strength and stirring speed during synthesis, which results in a high sticking efficiency, diffusion-limited coagulation, and consequently the formation of loose aggregates with low fractal dimension (*43*). While the open structure is maintained as long as the gel remains in water, removal of surface water by drying causes the open structure to collapse.

The pore structure of freeze-dried ferrihydrite has been extensively studied before (*27*, *30*, *44*). The average pore width as determined by gas adsorption ranged between 2 and 6 Å. We found that the dense aggregates maintained their structure even after several weeks of rehydration, suggesting that the compaction of aggregates by drying is irreversible and that their pore structure is very similar to that of dry samples. The persistence of the two morphologies in aqueous medium makes them suited to study the influence of their different pore structures on the sorption kinetics, similar to studies using alumina of varying particle and pore size distributions (*45*, *46*).

Sorption Kinetics. Both Cu and Pb showed a rapid sorption step, as indicated by the jump from 1 mmol/L to

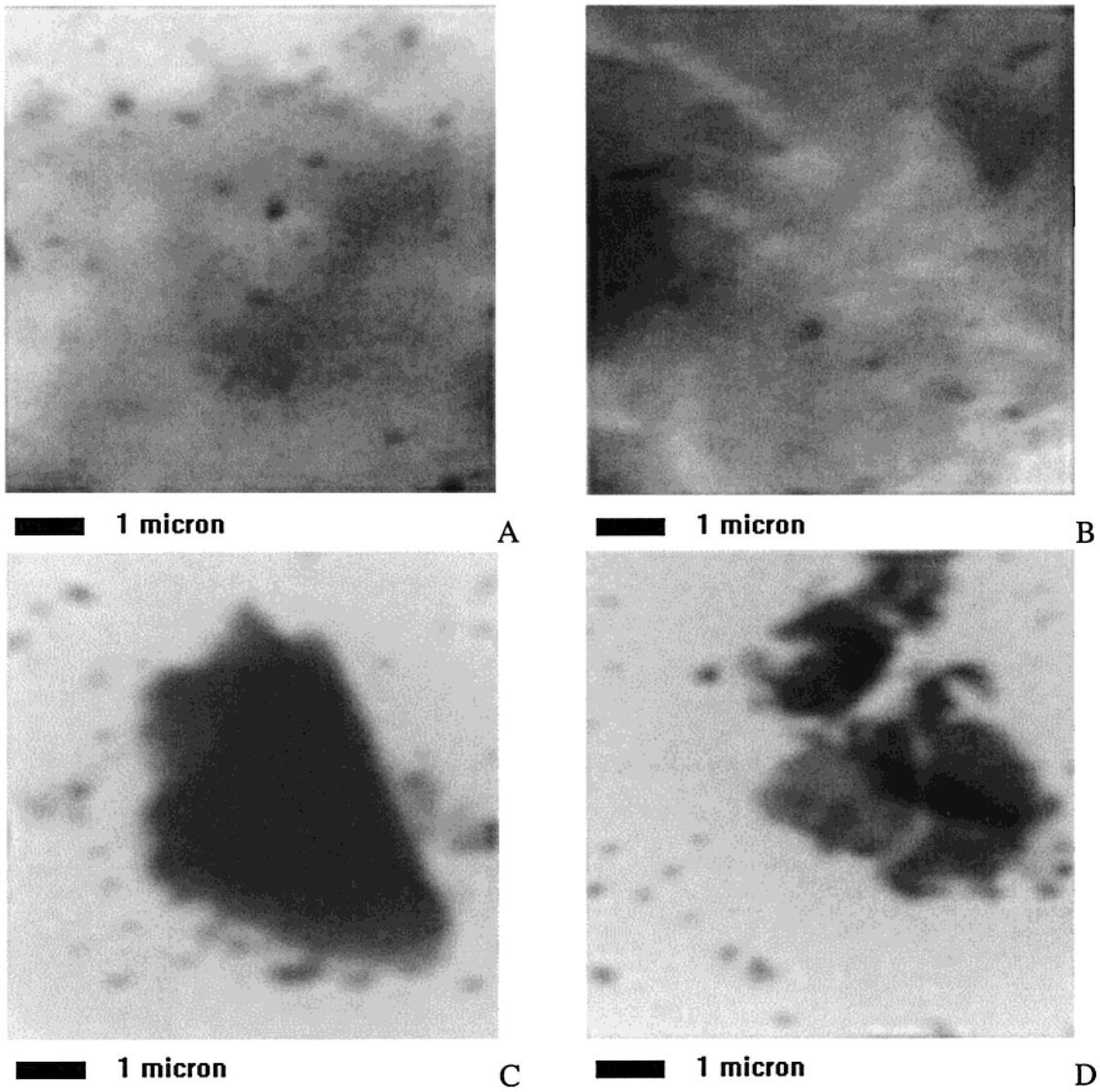

FIGURE 1. Scanning transmission X-ray micrographs of ferrihydrite suspended in 0.1 M $NaNO_3$ at pH 5. A and B show the gellike structure of a fresh ferrihydrite precipitate, while C and D show dense aggregates of freeze-dried and then rehydrated ferrihydrite. The images cover an area of 7.5 × 7.5 μm, collected with a step size of 30 nm and a dwell time of 25 ms/pixel.

the first data point after 5 min, followed by a slow step continuing for 2 months (Figure 2, top). Pb sorbed generally to a greater extent than Cu, in line with the higher affinity of Pb for ferrihydrite at pH 5 (*47*). Furthermore, both metals exhibited a greater affinity for ferrihydrite gel as compared to dense ferrihydrite. Temperature also had a remarkable influence on metal sorption (Figure 2, top). Cooling the system from 24 to 6 °C reduced both the initial amount of metal sorbed as well as the further sorption kinetics. In contrast to the strong effects of ferrihydrite pretreatment and temperature, the simultaneous addition of 1 mM Cu and 1 mM Pb had no significant influence on sorption kinetics, i.e., there was no competition between Cu and Pb (Figure 2, center). Suwannee River fulvic acid sorbed to the ferrihydrite surface also did not change sorption kinetics significantly (Figure 2, bottom). The relative contribution of slow sorption, operationally defined as the sorption between 5 min and 2 months, is compiled in Table 1. For ferrihydrite gel, slow sorption accounted for only 3% (Pb) and 13% (Cu), while it accounted for 43% (Pb) and 72% (Cu) of the total sorption to dense ferrihydrite.

Chemical Binding Mechanism. The χ(k) spectra and radial structure functions (RSFs) derived from Pb-edge XAFS are dominated by backscattering waves from two nearest oxygen neighbors at 2.3 Å (Figure 3, top, and Supporting Information). Despite the relatively high noise level typical for Pb-edge XAFS, the RSFs reveal a clear second-shell feature which could be fit with one iron neighbor at 3.3 Å. This configuration is consistent with the formation of a bidentate, edge-sharing sorption complex (*48*, *49*). This sorption complex was invariant as a function of time, ferrihydrite morphology, Cu adsorption, or presence of fulvic acid. The χ(k) spectra and RSFs of Cu-edge XAFS are dominated by backscattering waves from four nearest oxygen neighbors at 1.94 Å (Figure 3, bottom, and Supporting Information). These are the equatorial oxygens of the $Cu(OH)_6$ octahedron, which is distorted to remove the degeneracy of the Cu^{2+} (high-spin $3d^9$) electron ground state (*50*). We assume that the two axial oxygens at larger distance do not create an identifiable backscattering wave, either because the four closer equatorial oxygens shield them or because their distance from the central Cu atom is highly variable resulting in a high Debye−Waller factor. A relatively small second shell, marked with the hatched line in the RSFs, could be fitted with one iron neighbor at about 3.0 Å. This distance is within the range of the various edge-sharing configurations that are possible between the distorted $Cu(OH)_6$ octahedra and the more regular $Fe(OH)_6$ octahedra of ferrihydrite. Due to the much longer time necessary to

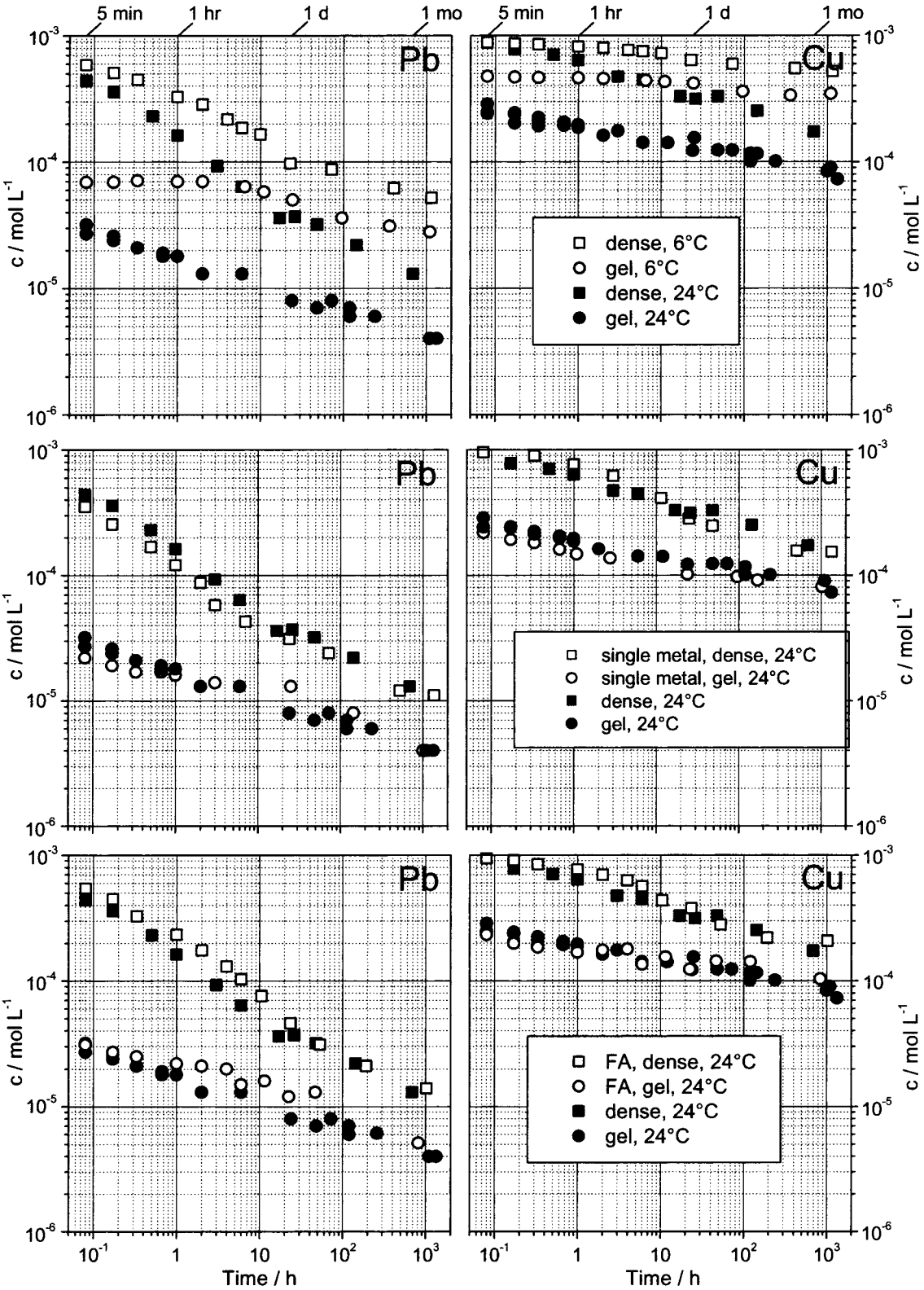

FIGURE 2. Kinetics of Pb and Cu removal from solution as influenced by ferrihydrite morphology ("dense" and "gel"), temperature (top), the absence of competing Cu or Pb cations ("single metal", middle), and the presence of Suwannee River fulvic acid ("FA", bottom). All data points represent systems with both metals present, except for the open symbols in the middle figure, where either Cu or Pb were sorbed.

collect useful Cu spectra, we investigated only four combinations of the variables ferrihydrite morphology, time, and metal competition. The results indicate that Cu, like Pb, binds only as bidentate, edge-sharing sorption complex at the experimental conditions of this study.

Mechanism of Slow Sorption. The chemical reaction leading to the formation of the observed inner-sphere sorption complexes may take place in milliseconds (*17*−*19*). Since we vigorously stirred the suspensions, it is unlikely that mass transport of metals through the free solution and

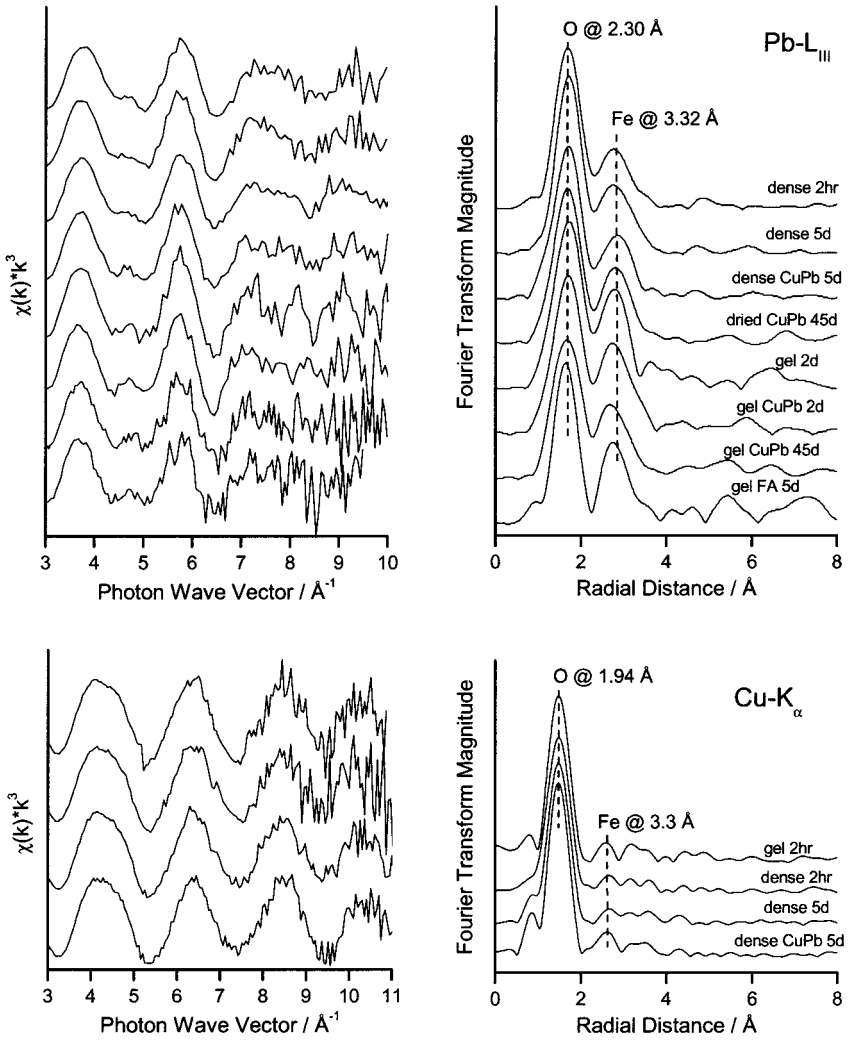

FIGURE 3. Pb−L$_{III}$ XAFS spectra (top) and Cu Kα XAFS spectra (bottom) of Pb and Cu sorbed onto ferrihydrite under various conditions as indicated by the labels. The weighed χ(k) functions (left) are shown in the same sequence as the labeled radial structure functions (right).

TABLE 1. Contribution of Slow Sorption (5 min to 2 months) to Total Sorption [%][a]

		Pb		Cu	
treatment		gel	dense	gel	dense
Cu + Pb	24 °C	2	43	20	80
Cu + Pb	6 °C	4	57	20	75
	24 °C	2	35	15	95
	6 °C	3	47	15	84
Cu + Pb, FA	24 °C	2	54	10	92
Cu + Pb, FA	6 °C	3	63	14	77
average		2	43	13	72

[a] Gel = gellike ferrihydrite aggregates; dense = dense ferrihydrite aggregates; Cu + Pb = both metals present; FA = fulvic acid.

the boundary layer around particles was rate limiting beyond 5 min. Furthermore, neither precipitation, coprecipitation, nor diffusion into the crystal lattice of ferrihydrite may explain the slow sorption, since we could exclude these processes by Pb- and Cu-edge XAFS. Even after 8 weeks reaction time at 24 °C, the XRD patterns of treated ferrihydrite samples showed only the two broad peaks of two-line ferrihydrite, excluding the possibility that ferrihydrite transformation may have been responsible for the observed slow sorption.

Therefore, limitation of the sorption reaction by surface diffusion toward "hidden" surface sites remains as the only explanation for the observed slow sorption. While ion diffusion through an aqueous medium is generally rapid (> mm/s), diffusion may slow by several orders of magnitude, when the water film at a reactive surface is thin compared to the size of an ion, because the ion then strongly interacts with the surface. A mean pore diameter of 2−6 Å observed for freeze-dried ferrihydrite (*27*, *30*, *44*) is in line with such a process. In contrast, the open structure of ferrihydrite gel may allow for fast access to all surface sites. The still significant amount of slow sorption into ferrihydrite gel may be due to surface diffusion into the smaller aggregates of medium density, which have been observed by STXM (Figure 1, A and B).

The observed temperature dependence of reaction kinetics may be used to estimate the relative contribution of diffusion to the observed sorption kinetics (*51*). To this end, we derived the activation energy of adsorption, *Ea*, from the Arrhenius equation. The calculation of *Ea* sensu stricto is not possible in our case, first, because our initial data points are relatively close to equilibrium and do not qualify for the derivation of first-order reaction rates and, second, because we determined the kinetics at only two temperatures (*52*). Still, *apparent* activation energies, E_{app}, may be derived to differentiate between diffusion-controlled reactions (smaller temperature-dependence, E_{app} < 42 kJ/mol) and reactions where the formation of the chemical bond is rate limiting (stronger temperature-dependence, E_{app} > 42 kJ/mol) (*51*).

TABLE 2. Apparent 5-min Rate Constants (k_{app}) at Two Temperatures, Collision Efficiencies (A), and Apparent Activation Energies for Adsorption (E_{app})

sorbate	sample	k_{app} 279 K	k_{app} 297 K	A [h^{-1}]	E_{app} [kJ/mol]
Pb	gel	0.66	2.58	3.88E+09	52
Pb	gel, FA	0.40	1.58	3.40E+09	53
Pb	dense	3.00	4.93	1.10E+04	19
Pb	dense, no Cu	3.23	5.39	1.51E+04	20
Pb	dense, FA	3.04	4.38	1.28E+03	14
Cu	gel	0.19	1.70	8.47E+14	84
Cu	gel, FA	0.19	1.56	1.97E+14	80
Cu	dense	0.44	1.72	2.16E+09	52
Cu	dense, no Pb	0.37	1.36	6.90E+08	50
Cu	dense, FA	0.42	1.32	6.75E+07	44

Since plots of log(c) over t were curved indicating an increasing back-reaction rate, we fitted the kinetic data of the first 30 min with a power law equation $c(t) = at^n$ and determined apparent rates, k_{app}, from the slope dc/dt at 5 min. As can be seen in Table 2, k_{app} generally decreased with temperature. However, E_{app} shows a higher temperature dependence of metal sorption on ferrihydrite gel compared to the sorption on dense ferrihydrite. Again, this in line with an easily accessible pore space of the gel and with surface diffusion into the small pores of the dense ferrihydrite. Also, the data show the insignificant influence of metal competition. While the observed trends of E_{app} are the same for Cu and Pb sorption, the absolute numbers are generally higher for Cu than for Pb. This may reflect the smaller size of the Cu^{2+} ions (87 pm) as compared to Pb^{2+} (143 pm) leading to less surface interaction at a given pore size.

Sorption of fulvic acid onto ferrihydrite was completed after 20 min, suggesting that fulvic acid molecules sorbed only to exterior surfaces. Consequently, ferrihydrite gel sorbed more fulvic acid (90%) than dense ferrihydrite with more restricted external surface sites (70%). However, after adding the metals, fulvic acid sorption increased to 94% and 85%, respectively, indicating that fulvic acid has a higher affinity for Cu and Pb sorbed at the ferrihydrite surface than for Fe in the ferrihydrite structure. Simultaneously, Cu and Pb seem to have a higher affinity for the ferrihydrite surface, otherwise the sorption of Cu and Pb would have decreased due to formation of soluble metal/fulvic acid complexes. This is further supported by the Pb-XAFS data, which show that Pb sorbed preferentially onto ferrihydrite even when fulvic acid was present. The only influence of fulvic acid on metal sorption manifested through a slightly lowered E_{app} for sorption on dense ferrihydrite. This may indicate that fulvic acid formed a diffusion barrier between the solution and the surface sites of ferrihydrite. Since we used a fulvic acid concentration of 100 mg/L typical for dissolved organic matter concentrations found in soil solution, this suggests that mainly the sorption behavior of minerals with a lower surface area than ferrihydrite is significantly influenced.

Cu and Pb form a similar type of sorption complex; hence, they most likely bind to the same sites at the ferrihydrite surface. Since the surface loadings achieved in our experiments correspond to only 1% of the total amount of available sites (assuming a sorption capacity of 1 mol metal per mole of Fe), competition effects are unlikely at longer sorption periods. However, our data show that competition is also not observable during the initial fast absorption, where accessible sorption sites are more limited.

Consequences of Slow Sorption for Modeling Metal Behavior. The long-term sorption by ferrihydrite drastically reduced metal concentrations in solution (Figure 2). Since ferrihydrite is present in many terrestrial and aquatic environments, surface diffusion is a process which has to be considered when predicting the fate of metals in the environment. The key controls of the reaction kinetics were ferrihydrite morphology and temperature. We assume that the two different types of ferrihydrite used in this study represent the extremes of ferrihydrite morphologies occurring in soils and sediments. In redoxomorphic soils or lake sediments, ferrihydrite gel forms at steep redox gradients due to fast precipitation. More consolidated ferrihydrite may form through seasonal drying of ferrihydrite gel or through slow precipitation. Furthermore, the temperature range between 6 and 24 °C may cover most reaction temperatures in natural environments. The quantification of diffusion-limited surface sites and the subsequent estimation of the effect of reaction time and temperature will be a challenge for properly predicting the fate of metals in the environment.

Acknowledgments

Supported by grants from the DuPont Co. and NSF. Annette Hofmann (ETHZ) measured the aggregate size distributions of the ferrihydrite suspensions. The group of Janos Kirz and Chris Jacobsen at SUNY Stony Brook developed the STXM at beamline X-1A, Brookhaven National Laboratory, with support from the Office of Biological and Environmental Research, U.S. DoE, under contract DE-FG02-89ER60858, and the NSF under grant DBI-9605045. Steve Spector and C. Jacobsen of Stony Brook and D. Tennant of Lucent Technologies Bell Labs developed the zone plates with support from the NSF under grant ECS-9510499.

Supporting Information Available

Two tables with the results of the Pb−L_{III} XAFS and the Cu−K XAFS fits (2 pages). This material is available free of charge via the Internet at http://pubs.acs.org.

Literature Cited

(1) Cornell, R. M.; Schwertmann, U. *The iron oxides: Structure, properties, reactions, occurrence and uses*; VCH Verlagsgesellschaft: Weinheim, 1996.
(2) Jambor, J. L.; Dutrizac, J. E. *Chem. Rev.* **1998**, *98*, 2549−2585.
(3) Schwertmann, U.; Cambier, P.; Murad, E. *Clays Clay Miner.* **1985**, *33*, 369−378.
(4) Cornell, R. M.; Schwertmann, U. *Clays Clay Miner.* **1979**, *27*, 402−410.
(5) Cornell, R. M.; Giovanoli, R.; Schindler, P. W. *Clays Clay Miner.* **1987**, *35*, 21−28.
(6) Cornell, R. M. *Z. Pflanzenernaehr. Bodenkd.* **1987**, *150*, 304−307.
(7) Cornell, R. M.; Giovanoli, R.; Schneider, W. *J. Chem. Technol. Biotechnol.* **1992**, *53*, 73−79.
(8) Manceau, A.; Gates, W. P. *Clays Clay Miner.* **1997**, *45*, 448−460.
(9) Dzombak, D. A.; Morel, F. M. M. *Surface complexation modeling. Hydrous ferric oxide*; John Wiley & Sons: New York, 1990.
(10) Waychunas, G. A.; Rea, B. A.; Fuller, C. C.; Davis, J. A. *Geochim. Cosmochim. Acta* **1993**, *57*, 2251−2269.
(11) Eggleton, R. A.; Fitzpatrick, R. *Clays Clay Miner.* **1988**, *36*, 111−124.
(12) Waychunas, G. A.; Fuller, C. C.; Rea, B. A.; Davis, J. A. *Geochim. Cosmochim. Acta* **1996**, *60*, 1765−1781.
(13) Charlet, L.; Manceau, A. *J. Colloid Interface Sci.* **1992**, *148*, 443−458.
(14) Waychunas, G. A.; Davis, J. A.; Jutson, J. A.; Fuller, C. C. *Geochim. Cosmochim. Acta* **1995**, *59*, 3655−3661.
(15) Manceau, A.; Charlet, L. *J. Colloid Interface Sci.* **1994**, *168*, 87−93.
(16) Spadini, L.; Manceau, A.; Schindler, P. W.; Charlet, L. *J. Colloid Interface Sci.* **1994**, *168*, 73−86.
(17) Hachiya, K.; Sasaki, M.; Ikeda, T.; Mikami, N.; Yasunaga, T. *J. Phys. Chem.-US* **1984**, *88*, 27−31.
(18) Zhang, P. C.; Sparks, D. L. *Soil Sci. Soc. Am. J.* **1989**, *53*, 1028−1034.
(19) Grossl, P. R.; Sparks, D. L.; Ainsworth, C. C. *Environ. Sci. Technol.* **1994**, *28*, 1422−1429.
(20) McBride, M. B. *Environmental Chemistry of Soils*; Oxford University Press: New York, 1994.

(21) Van Riemsdijk, W. H.; Boumans, L. J. M.; De Haan, F. A. M. *Soil Sci. Soc. Am. J.* **1984**, *48*, 537−541.
(22) Dzombak, D. A.; Morel, F. M. M. *J. Colloid Interface Sci.* **1986**, *112*, 588−598.
(23) Ainsworth, C. C.; Pilon, J. L.; Gassman, P. L.; Van Der Sluys, W. G. *Soil Sci. Soc. Am. J.* **1994**, *58*, 1615−1623.
(24) Ford, R. G.; Bertsch, P. M.; Farley, K. J. *Environ. Sci. Technol.* **1997**, *31*, 2028−2033.
(25) Ford, R. G.; Kemner, K. M.; Bertsch, P. M. *Geochim. Cosmochim. Acta* **1999**, *63*, 39−48.
(26) Fuller, C. C.; Davis, J. A.; Waychunas, G. A. *Geochim. Cosmochim. Acta* **1993**, *57*, 2271−2282.
(27) Axe, L.; Anderson, P. R. *J. Colloid Interface Sci.* **1995**, *175*, 157−165.
(28) Axe, L.; Anderson, P. R. *J. Colloid Interface Sci.* **1997**, *185*, 436−448.
(29) Willett, I. R.; Chartres, C. J.; Nguyen, T. T. *J. Soil Sci.* **1988**, *39*, 275−282.
(30) Bottero, J.-Y.; Arnaud, M.; Villieras, F.; Michot, L. J.; De Donato, P.; Francois, M. *J. Colloid Interface Sci.* **1993**, *159*, 45−52.
(31) Schwertmann, U.; Cornell, R. M. *Iron Oxides in the Laboratory: Preparation and Characterization*, 2nd ed.; VCH Verlagsgesellschaft: New York, 2000.
(32) Borken, W.; Xu, Y.-J.; Brumme, R.; Lamersdorf, N. *Soil Sci. Soc. Am. J.* **1999**, *63*, 1848−1855.
(33) Rover, M.; Kaiser, E. A. *Soil Biol. Biochem.* **1999**, *31*, 175−187.
(34) Kaiser, K.; Zech, W. *Soil Sci.* **1998**, *163*, 714−725.
(35) Jacobsen, C.; Williams, S.; Anderson, E.; Browne, M. T.; Buckley, C. J.; Kern, D.; Kirz, J.; Rivers, M.; Zhang, X. *Opt. Commun.* **1991**, *86*, 351−364.
(36) Spector, S.; Jacobsen, C.; Tennant, D. *J. Vacuum Sci. Technol. B* **1997**, *15*, 2872−2876.
(37) Neuhäusler, U.; Jacobsen, C.; Schulze, D.; Stott, D.; Abend, S. *J. Synchrotron Radiat.* **2000**, *7*, 110−112.
(38) Ressler, T. *J. Synchrotron Radiat.* **1998**, *5*, 118−122.
(39) Rehr, J. J.; Mustre de Leon, J.; Zabinsky, S.; Albers, R. C. *J. Am. Chem. Soc.* **1991**, *113*, 5135−5140.
(40) Oswald, H. R.; Reller, A.; Schmalle, H. W.; Dubler, E. *Acta Crystallogr.* **1990**, *C46*, 2279−2284.
(41) Leciejewicz, J. *Acta Crystallogr.* **1961**, *14*, 1304.
(42) Tchoubar, D.; Bottero, J.-Y.; Quienne, P.; Arnaud, M. *Langmuir* **1991**, *7*, 398−402.
(43) Buffle, J.; Leppard, G. G. *Environ. Sci. Technol.* **1995**, *29*, 2169−2175.
(44) Weidler, P. G.; Stanjek, H. *Clay Miner.* **1998**, *33*, 277−284.
(45) Papelis, C.; Roberts, P. V.; Leckie, J. O. *Environ. Sci. Technol.* **1995**, *29*, 1099−1108.
(46) Michard, P.; Guibal, E.; Vincent, T.; LeCloirec, P. *Microporous Mater.* **1996**, *5*, 309−324.
(47) McKenzie, R. M. *Aust. J. Soil Res.* **1980**, *18*, 61−73.
(48) Manceau, A.; Charlet, L.; Boisset, M. C.; Didier, B.; Spadini, L. *Appl. Clay Sci.* **1992**, *7*, 201−223.
(49) Bargar, J. R.; Brown, G. E., Jr.; Parks, G. A. *Geochim. Cosmochim. Acta* **1997**, *61*, 2639−2652.
(50) Burns, R. G. *Mineralogical Applications of Crystal Field Theory*, 2nd ed.; Cambridge University Press: New York, 1993.
(51) Sparks, D. L. *Kinetics of Soil Chemical Processes*; Academic Press: New York, 1989.
(52) Espenson, J. H. *Chemical Kinetics and Reaction Mechanisms*, 2nd ed.; McGraw-Hill: New York, 1995.

Received for review May 23, 2000. Revised manuscript received December 11, 2000. Accepted December 18, 2000.

ES000107M